Double-well potential energy surface in the interaction between *h*-BN and Ni(111)

*Jorge Ontaneda,[1,2] Francesc Viñes,[3] Francesc Illas,[3] Ricardo Grau-Crespo[1]**

[1]Department of Chemistry, University of Reading, Whiteknights, Reading RG6 6AD, UK.

[2]Departamento de Química, Universidad Técnica Particular de Loja, San Cayetano Alto, Loja 1101608, Ecuador.

[3]Departament de Ciència de Materials i Química Física & Institut de Química Teòrica i Computacional (IQTCUB), Universitat de Barcelona,
c/ Martí i Franquès 1, 08028, Barcelona, Spain.

Email: r.grau-crespo@reading.ac.uk

Abstract. Density functional theory calculations with non-local correlation functionals, properly accounting for dispersion forces, predict the presence of two minima in the interaction energy between *h*-BN and Ni(111). These can be described as a physisorbed state with no corrugation of the *h*-BN structure, and a chemisorbed state exhibiting noticeable corrugation and shorter distance of *h*-BN to the metallic support. The latter corresponds indeed to the one reported in most experiments. The relative stability of the two minima depends on the specific density functional employed: of those investigated here only the optB86b-vdW yields the correct order of stability. We also demonstrate that the effect of the

metal support on the Raman frequency of the chemisorbed boron nitride monolayer cannot be reduced to the associated strain. This is important because the Raman frequency has been proposed as a signature to identify *h*-BN monolayers from multilayered samples. Our analysis shows that such signatures would be strongly dependent on the nature of the support – *h*-BN interaction.

Keywords: hexagonal boron nitride; Ni(111); dispersion interactions; density functional theory.

1. INTRODUCTION

In the last two decades, the epitaxial growth of few-layers of hexagonal boron nitride (*h*-BN) on the (111) surface of face-centered cubic (*fcc*) metals such as Au, Cu, Rh, Pt, Pd, Ir, and Ni has been widely studied.[1–9] The motivation for these studies is that *h*-BN/metal interfaces have potential applications in areas such as protective coating, transparent membranes, or deep ultraviolet emitters.[10–12] Recent theoretical investigations have also suggested that metal-supported nanosheets of *h*-BN might be active for both CO oxidation and oxygen reduction reaction (ORR).[13,14] Indeed, the combined experimental and theoretical study of Uosaki *et al.* demonstrated that *h*-BN supported on Au(111) surface has much better catalytic activity for ORR than a pure Au(111) electrode.[2] These authors suggested that defective *h*-BN nanosheets with edge sites play an important role in the ORR. The theoretical work of Gao and coworkers[15] showed that the energy barrier for the ORR depends on the type of defects, which also play an important role at enhancing the stability the *h*-BN/metal heterostructures.

The interaction between *h*-BN and metal surfaces is complex even in the absence of defects, as it involves strain effects, dispersion interactions, and electronic redistribution. Early experimental studies by Rokuta *et al.* demonstrated that orbital hybridization at the Ni(111) and *h*-BN nanosheets interface generates metallic bands.[16] Other transition metal substrates, including Rh(111) and Pt(111) surfaces, have been also reported to modify the electronic properties of supported *h*-BN in a similar way.[17,18] Theoretical studies have suggested that the metallic behavior of *h*-BN when supported on metal substrates can be due to the mixing of *d* orbitals of the metal with the 2*p* orbitals of N and B of *h*-BN.[2,19]

The Ni(111) surface is an interesting substrate for atomically-thin layers of *h*-BN since the lattice constant of the former (249 pm)[20] almost perfectly matches that of the latter (251 pm), *i.e.*, their degree of incommensurability is below 0.8%.[21] It has been suggested that the *h*-BN monolayer on Ni(111) overcomes the small lattice mismatch by introducing a slightly rumpled structure, allowing the formation of a commensurate $p(1\times1)$ system.[16] Most of the recent theoretical work about this interface has been devoted to the catalytic activity towards the CO oxidation and ORR.[13,15] In these studies, the dispersion has been treated empirically under the so-called D2 method on top of semi-local density functionals (in the generalized gradient approximation), which may miss relevant features. Here, we investigate the interface geometry and electronic structure of *h*-BN layers supported on the Ni(111) surface using non-local correlation functionals, optB88-vdW and optB86b-vdW, which offer more robust descriptions of dispersion interactions. We will show that a double-well potential energy surface exists for the interaction of *h*-BN with the metal support, with two minima that can be identified as chemisorption and physisorption states, respectively. In addition, we discuss the effect of the Ni support on the Raman signal of *h*-BN, which is important given that Raman peaks can be used experimentally to identify the presence of *h*-BN monolayers, in contrast with *h*-BN bulk.[22]

2. COMPUTATIONAL METHODS

Density functional theory (DFT) calculations were carried out using plane wave basis sets as implemented in the VASP code.[23,24] The projected augmented wave (PAW) method[25,26] was used to describe the effect of core electron on the valence electron density. The number of plane waves in the calculations was limited by a kinetic energy cutoff of 410 eV. In order to sample the Brillouin zone, a Monkhorst-Pack[27] **k**-point grid of 7×7×1 was used throughout the simulations involving the metal slabs. The Methfessel-Paxton smearing method of first order was used with an energy width of $\sigma = 0.2$ eV; total energies were extrapolated to $\sigma=0$. For the calculation of densities of states (DOS) we used the tetrahedron method with Blöchl corrections. The threshold for forces acting on ions was set to 0.005 eV $Å^{-1}$. Test calculations with a lower threshold, of 0.001 eV $Å^{-1}$, led to zero or negligible effect on the computed interaction energies, corrugation and separation between the Ni substrate and the monolayer. To compensate for the use of an asymmetric slab, all simulations included a dipole correction as implemented in VASP, based on a method proposed by Makov and Payne.[28]

Following the approach of a previous DFT investigation of graphene on this metal substrate,[29] the Ni(111) surface was modeled with a periodic slab of six atomic layers. Only the three uppermost Ni layers were fully relaxed, while the three bottom layers were fixed in their bulk positions. The adsorption of *h*-BN on a Ni(111) surface was investigated employing a small *p*(1×1) supercell containing one N atom and one B atom; this model was observed in the *p*(1×1) LEED pattern in Ref. 30. A wide vacuum gap of 20 Å was included in order to avoid interactions between slabs. As nickel is a ferromagnetic metal, all calculations included spin polarization.

We compared results obtained from calculations with various functionals including the generalized gradient approximation (GGA) in the formulation by Perdew-Burke-Ernzerhof

(PBE),[31] as well as their empirical corrections by Grimme's method (D2 and D3)[32,33] to account for dispersion. We also consider the optB88-vdW and optB86b-vdW functionals where dispersion is treated with explicit non-local correlation,[34] as developed and implemented in VASP by Klimeš *et al.*[35]

The interaction energy (E_{int}) of *h*-BN adsorbed on the Ni(111) surface was computed as:

$$E_{\mathrm{int}} = E_{\mathrm{interface}} - (nE_{h-\mathrm{BN}} + E_{\mathrm{surf}}), \quad (1)$$

where $E_{\mathrm{interface}}$ is the total energy of the *h*-BN/Ni(111) slab, including *n* formula units of *h*-BN; $E_{h\text{-BN}}$ is the energy per formula unit of a free-standing (unstrained) *h*-BN sheet, and E_{surf} is the total energy of the clean Ni(111) slab.

The energy barrier and potential energy surface between the chemisorption and physisorption minima was obtained using the nudged elastic band method.[36] This method works by optimizing a number of intermediate images along a reaction coordinate, which in our case was the average (vertical) separation between the Ni substrate and the *h*-BN layer, under the constraint of equal spacing between neighboring images.

3. RESULTS

In the commensurate system of *h*-BN on Ni substrate, N and B can be expected to occupy high-symmetry points on top of the Ni(111) surface unit cell. Early experiments[9,30] and recent theoretical work[13,15,37] considered three high-symmetry sites (*top*, *fcc*, and *hcp*) at the Ni(111) surface for the exploration of the equilibrium interface geometries of the *h*-BN/Ni(111) structure. In a similar system, graphene on Ni(111) surfaces, high-resolution X-ray photoelectron spectroscopy (HR-XPS) have detected the coexistence of *bridge* and *top-fcc*

structures.[29] Hence, we have also considered *bridge* geometries, where the B-N bond sits on *top*, *fcc*, and *hcp* sites, generating three additional arrangements. Due to the presence of two atomic species in the monolayer, two non-equivalent interfaces can be formed, which we call *Interface A* and *Interface B.* These interfaces cannot be converted into one another by a simple translation. As a result, twelve high-symmetry configurations/interfaces were explicitly considered, six for each interface (**Figure 1**).

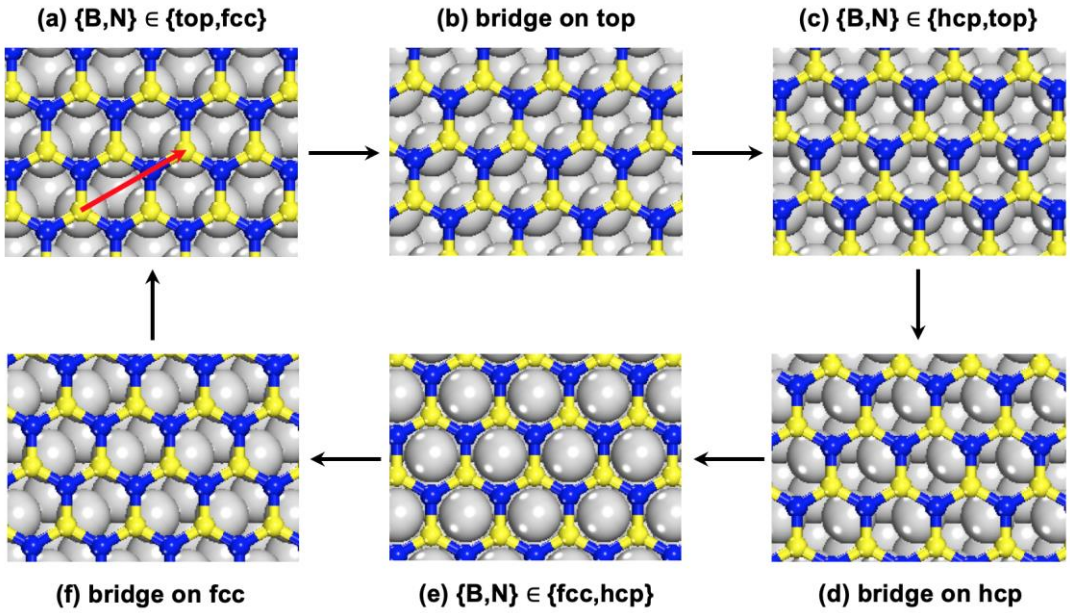

Figure 1. Six different arrangements for the *h*-BN monolayer on the Ni(111) surface. The configurations are related to each other by a small displacement of the *h*-BN monolayer relative to the Ni(111) surface in the direction indicated by the red arrow in panel (a), *e.g.* along a B-N bond. The magnitude of a full displacement is 429.5 pm (red arrow). The scheme shown here corresponds to *Interface A*; by swapping the positions of B and N, *Interface B* is obtained. Key: light grey = Ni, yellow = B, and blue = N.

For each one of these model systems, the potential energy surface was explored by fixing the lateral position of the *h*-BN atoms while letting the vertical distance from the Ni(111) plane to relax. Nevertheless, final simulations of the most stable configurations are carried out removing all constraints.

The optB88-vdW potential surface energy plot (**Figure 2a**) reveals two local minima for the equilibrium interface geometry between the *h*-BN monolayer and Ni(111) surface. According to **Figure 2a**, the most stable structures are formed when N atoms are on the *top* position. The B atoms, on the other hand, have two possible situations on the Ni surface: on *hcp* (found in the set of *Interface A* geometries) and on *fcc* (*Interface B*). Both conformations are energetically equivalent and equally located by the present DFT calculations within the optB88-vdW method: B on *hcp* position is marginally less stable than B on *fcc* by 0.3 meV/atom. This is consistent with early X-ray photoelectron diffraction (XPD) and scanning tunneling microscope (STM) measurements which found that both configurations can coexist, separated by a line defect.[9,38,39] The remaining configurations are not minima of the potential energy surface. Note also that those configurations where the B-N bond is in a bridge on *top*, on *hcp*, and on *fcc* site, spontaneously evolved into either *top-hcp* or *top-fcc* when lateral constraints were not imposed.

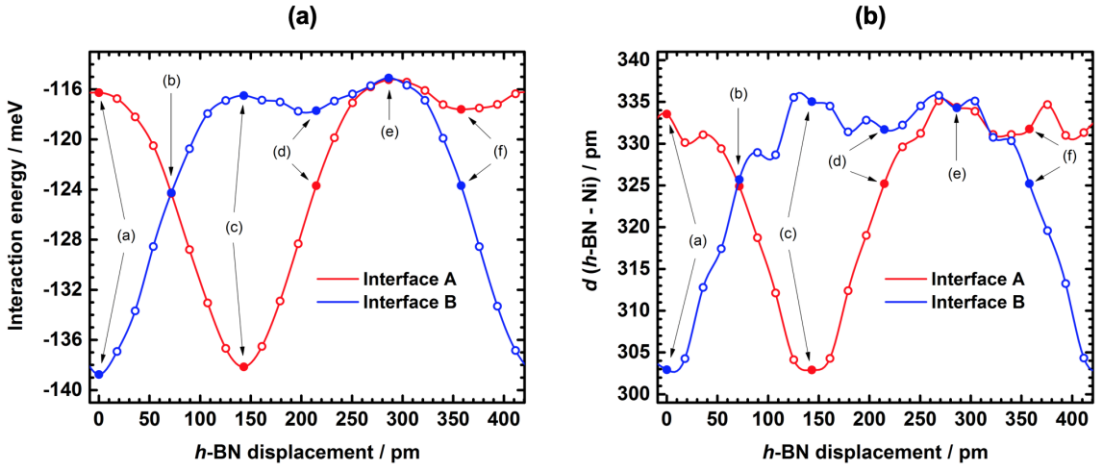

Figure 2. (a) Potential energy surface (per BN formula unit) and (b) average distance *d* between the *h*-BN monolayer and the Ni(111), when going from configuration (a) to (f) along the B-N bond following the red arrow and the notation in Figure 1. The filled circles represent high-symmetry configurations, and the empty circles represent intermediate configurations (shifted by a displacement of ~17.9 pm.

For the most stable configuration found (N on *top*, B on *fcc* for *Interface B*), the calculated average distance between *h*-BN and Ni(111) is 303 pm (see **Figure 2b**). The *h*-BN is practically flat: N and B atoms are almost equally separated from the Ni surface, with the maximum difference in height between N and B being 0.9 pm (B atoms slightly closer to the substrate). These observations, together with the relatively small value predicted for the interaction energy (~69 meV/atom), lead us to interpret this configuration as a physisorption state, *i.e.* the interface binding is mainly due to van der Waals interactions. In comparison, the interaction energy predicted in Ref. 40 (using the same functional) for the physisorbed graphene/Ni(111) system was 51 meV/atom. However, in that work it was reported that chemisorbed states also existed, even though the optB88-vdW functional incorrectly predicted them as less stable than physisorbed states, whereas the optB86b-vdW was able to give the correct relative stabilities. We therefore need to investigate whether the same situation is present in the optB88-vdW description of the *h*-BN/Ni(111) system, *i.e.* whether the present approach is able to capture the chemisorbed states.

In this context, we briefly discuss the experimental and theoretical evidence about the *h*-BN/Ni(111) from previous studies. Early LEED measurements by Gamou *et al.*[30] determined an interface structure with the nitrogen atoms on *top* sites, and boron atoms are at the *fcc* sites, similarly to what we found to be the lowest energy configuration. However, in that experimental study, the perpendicular spacing between B (N) and the topmost Ni was found to be 204 pm (222 pm), giving a corrugation value of 18 pm for the supported *h*-BN monolayer. Later XPD studies by Auwärter and coworkers[9] reported the same interface geometry but with a lower corrugation value, 7±6 pm. In recent transmission electron microscopy (TEM) measurements Tonkikh *et al.*[37] reported a *h*-BN monolayer-Ni separation of 187±12 pm. Therefore, most experimental determinations of the interface geometry suggest the occurrence of chemisorbed states. Only the early work of Nagashima and

coworkers, via angle-resolved electron spectroscopic methods, argued that the adsorption state was physisorbed.[41–44] On the theory side, Grad *et al.*,[45] using a GGA functional, found a chemisorbed configuration in which a corrugated *h*-BN layer was found at 208 pm (for B) and 219 pm (for N) with respect to the Ni surface. Similarly, Laskowski *et al*.[46] reported the existence of a corrugated layer of *h*-BN when supported on Ni(111). In this study, the equilibrium separations between the BN layer and the Ni surface were 212-214 pm, in both local density approximation (LDA) and GGA calculations. On the other hand, Huda *et al.*[47] found adsorption distances of the BN monolayers on the Ni(111) surfaces in the range of 350–400 pm, using GGA calculations. However, by repeating the calculations using the LDA, these authors found a chemisorbed state whose properties (buckling and separation) are in good agreement with experiment,[47] although this result could be affected by the well-known overbinding trend of the LDA. Simulations with Grimme-corrected PBE functionals have also identified chemisorbed states for this interface.[13,15,37] Using a non-local correlation functional, Ebnonnasir *et al.*[48] found two adsorption configurations of *h*-BN on Ni(111), one chemical and one physical. Clearly, no consensus about the nature of the interaction has been reached yet.

In our study, the initial automatic search with the optB88-vdW method, as described above, found only physisorbed states (**Figure 2**). However, if we start from the same N(*top*)-B(*fcc*) configuration, but *manually* placing the monolayer closer to the Ni substrate and relaxing the ions using a less aggressive optimizer (we used the quasi-Newton method), the optB88-vdW simulation was able to converge to a minimum at shorter distances. In this local minimum, the corrugation value is estimated as 7.2 pm with the B atom closer to Ni substrate, in good agreement with the XPD measurements.[9] Moreover, the interlayer separation *h*-BN monolayer-Ni as 221 pm, in line with LEED[30] and TEM[37] reports. The geometry of this interface configuration thus corresponds to a chemisorbed state, even if it

has a weaker interaction (by ~10 meV/atom) than the physisorbed state calculated with the same functional. In order to understand the relationship between the two minima, we also investigated the transition from one to the other using the nudged band elastic (NEB) method (**Figure 3)**. The two minima are separated by a small energy barrier of ~1.6 meV/atom.

The coexistence of two minima in the potential energy surface, one corresponding to a physisorbed state, at a longer distance and with little corrugation, and one corresponding to a chemisorbed state, at shorter distance and with significant corrugation, is physically plausible. For example, it has been recently found that two distinguishable adsorption wells coexist at the interface between graphene and silicon oxide, although in that case the chemisorption well was reached experimentally only under ultra-high pressure.[49] In the same way, it is possible that the two wells of the h-BN/Ni(111) interface could be accessible under different experimental conditions, which would require further investigation. However, the relative energies of the two minima predicted by the optB88-vdW are unlikely to be correct, as one should expect chemical interactions to lead to stronger adsorption than dispersion interactions. The result is probably an artifact from the use of the optB88-vdW functional, as observed by Janthon *et al.*[40] in the description of the graphene/Ni(111) interface. These authors also found that the optB86b-vdW functional does lead to the expected behavior, clearly favoring chemisorption over physisorption on Ni(111), and also providing a correct description for geometries and adsorption energies of chemisorbed and physisorbed states.

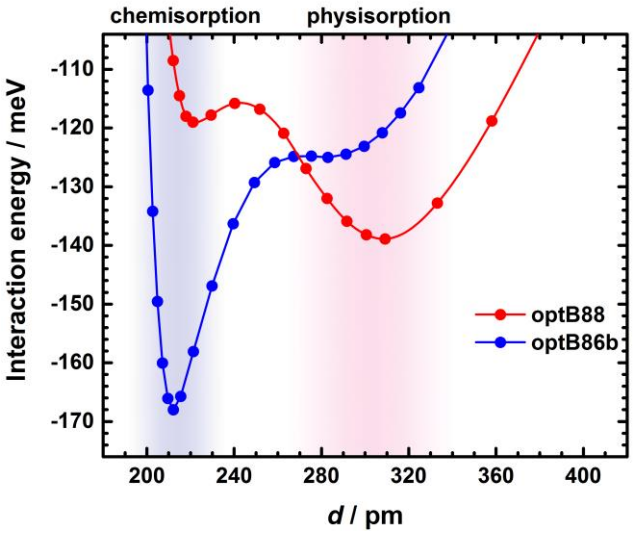

Figure 3. Interaction energies (per BN formula unit) as functions of the average separation *d* between the Ni substrate and the *h*-BN monolayer, as calculated for the N(*top*)-B(*fcc*) configuration, using the optB88-vdW and optB86b-vdW functionals. The saddle points were located by means of nudged elastic band calculations.

We have therefore investigated the relative adsorption strength at the chemisorbed and physisorbed states for the *h*-BN/Ni(111) system with the optB86b-vdW functional, as well as with the empirically-corrected (Grimme's) functionals PBE-D2 and PBE-D3, and the results are listed in **Table 1**. Interestingly, all these functionals predict the existence of both local minima thus reinforcing the present theoretical prediction. Moreover, the formation of the interface, in either the physisorbed or chemisorbed state, is energetically favorable (negative formation energy) for all functionals except for PBE, which does not account for the stabilizing dispersion interactions, and thus incorrectly lets the strain effect to dominate. Interestingly, the only functional that correctly identifies the chemisorbed state as more stable than the physisorbed state is the optB86b-vdW functional, as observed for graphene/Ni(111). In fact, this functional predicts a very shallow physisorbed minimum, with a barrier of less than 0.1 meV/atom to transit to the chemisorbed minimum (**Figure 3**). In future work, it would be interesting to also test other recently developed functionals, like the PBE-vdW^{surf}

functional, which can account for the nonlocal screening within the bulk.[50] However, recent investigations of molecular adsorption at metal surfaces[51,52] have shown that the PBE+vdW^{surf} and the optB88-vdW functionals, while based on different approximations, lead to nearly equivalent quantitative agreement in adsorption energies and equilibrium distances.

Table 1. Average interlayer separation (d), corrugation and interaction energies (E_{int}) of the chemisorbed and physisorbed interface geometries for the *h*-BN/Ni(111) system, according to the listed functionals. Average interlayer separation and corrugation values are given in pm, and interaction energies are given in meV/atom.

Functional	**Chemisorption**			**Physisorption**		
	d	**corrugation**	E_{int}	d	**corrugation**	E_{int}
PBE	211	10.3	11.1	413	0.1	3.4
PBE-D2	209	11.3	-54.9	281	2.2	-88.3
PBE-D3	214	10.4	-29.4	303	1.4	-68.8
optB88-vdW	221	7.2	-59.5	303	0.9	-69.5
optB86b-vdW	212	9.9	-84.1	282	1.9	-62.5
Exp	213[a]	18[a]				
	187±12[b]	7±6[c]				

[a] Ref. 30; [b] Ref.37; [c] Ref. 9

The optB88-vdW functional, which in Ref. [53] we found to be particularly good in the description of free-standing *h*-BN, can lead to a chemisorbed minimum for *h*-BN on Ni(111), although it does not identify it as the most favorable minimum for adsorption. For compatibility with our previous work where we investigated the origin of Raman signature in monolayers of *h*-BN,[53] we will discuss below the addition of extra layers and the Raman

frequencies of supported *h*-BN as calculated with the optB88-vdW (at the correct chemisorbed minimum), such that it facilitates the comparison between the free-standing and supported systems.

Table 2. Average interlayer separation (*d*) and interaction energy (E_{int}) of few-layer of *h*-BN on Ni(111) surface. Interlayer separation is given in pm and interaction energy in meV/atom.

System	Interlayer separation *d*			E_{int}
	Ni - 1st layer	1st - 2nd layer	2nd – 3rd layer	
1 ML	221	-	-	-59.5
2 ML	221	327	-	-61.6
3 ML	221	325	330	-60.9

Table 2 shows the optimization results of few-layers, up to 3 ML, of *h*-BN on the Ni(111) surface. The formation of the interface is slightly more favorable in the presence of extra *h*-BN layers. The shorter interlayer distance at the interface suggest that the first layer of *h*-BN might have different electronic properties compared to the next layers. Experimental studies by Rokuta *et al.*[16] have indeed demonstrated that orbital hybridization at the Ni(111) and *h*-BN nanosheets interface generates metallic bands. The experimental work on *h*-BN multilayers on Ni(111) by Tonkikh and coworkers[37] also reports that the first *h*-BN layer at the interface to Ni is metallic. Furthermore, these authors found a decoupling of the second layer from the underlying substrate, which leads to the restoration of the insulating nature of *h*-BN system. The computed density of states (DOS) projected on *h*-BN (**Figure 4**) follows the same trend, in agreement with the experiment reported in Ref. 37: the interface layer exhibits a metallic behavior whereas the surface layer (and second layer in case of the tri-

layer system) has the same features to that of a free-standing (unstrained) BN sheet. For the supported monolayer, a Bader charge population analysis shows a small but significant net transfer of 0.04 *e* (per BN formula unit), which mainly takes place from the Ni top layer to the boron sublattice (which is closer to the Ni surface than the N sublattice). The charge transfer is expected to occur given the band alignment before contact (by aligning the two systems separately with the vacuum level we obtain that the Fermi level of the metal is more than 1 eV about the top of the valence band of *h*-BN) and the strong hybridization of orbitals from both sides of the interface, which creates available states in *h*-BN.

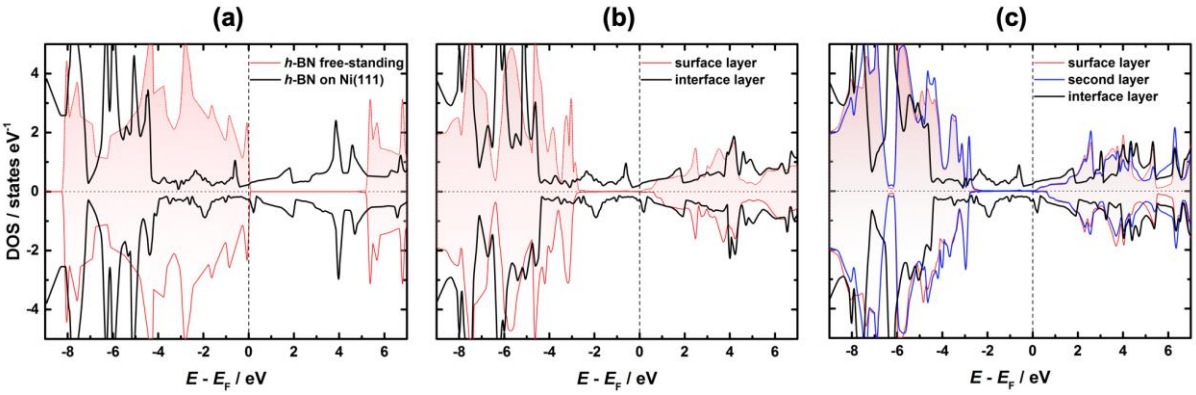

Figure 4. Layer-resolved electronic density of sates (DOS) for (a) mono-, (b) bi-, and (c) tri-layers of *h*-BN supported on Ni(111) surface. Panel (a) exhibits also the DOS computed for a free-standing (unstrained) monolayer.

Finally, we discuss the calculated Raman frequency of the metal-supported *h*-BN monolayer (1421.5 cm^{-1}) in comparison with that of the free-standing, flat *h*-BN monolayer (1333.1 cm^{-1}) at its equilibrium cell parameter. The value for the supported system is much larger, which is partially expected from the findings presented in our recent work:[53] the in-plane compression associated to the interface formation should lead to an increase in the frequency of the in-plane modes. However, the difference (88.4 cm^{-1}) cannot be explained only based on the associated contraction (*indirect* effect). In fact, a simple computational experiment finds that the Raman frequency of a free-standing *h*-BN layer compressed to

match the cell parameter of Ni(111) is 1402.0 cm^{-1}, which is still 19.5 cm^{-1} below the value for the Ni-supported monolayer. This result provides compelling evidence of a *direct* support-induced effect, which contributes to the Raman frequency upshift. The direct effect includes charge transfer, which alters the rigidity of the in-plane *h*-BN bonds. However, charge transfer alone is not enough either to explain the addition Raman upshift either: an auxiliary calculation of the unsupported monolayer with the compressed cell parameter *and* the additional electron charge of 0.04 per formula unit (compensated by a uniform positive charge background), yields a frequency of 1406.0 cm^{-1}. Other specific details of the interaction between BN and the Ni support, including charge polarization and geometric distortion (corrugation), affect the value of the Raman frequency.

Our findings are important for understanding the Raman signature of *h*-BN monolayers in supported systems. We have previously shown that there is a small intrinsic signature,[53] but support-induced effects appear to be significant. The present results highlight the complex role of the support, which cannot be simply reduced to interface strain effects. In fact, the present model calculations evidence that direct interactions, in the form of charge transfer, polarization and chemisorption, significantly contribute to the magnitude of the Raman shift. Therefore, a detailed understanding of the nature of the *h*-BN/support interaction is necessary to elucidate the origin of Raman shifts in specific supported *h*-BN systems.

4. CONCLUSIONS

In summary, we have shown that non-local correlation functionals predict the presence of two minima in the interaction energy between *h*-BN and Ni(111): one geometrically flat that can be identified as a physisorbed state and one with appreciable corrugation of the *h*-BN lattice and shorter interface distance, which can be identified as a chemisorbed state. Both empirically-corrected GGA functionals and non-local correlation functionals can locate the

two minima in the potential energy surface, but only the optB86b-vdW is able to give the correct order of stability.

In the chemisorbed state, which is the one reported in most experiments, there is significant charge transfer from Ni to *h*-BN, which becomes metallic. We have found that the large increase in the Raman frequency of the supported *h*-BN is due to a combination of lattice contraction associated with the interface formation (*indirect* effects) and the interaction with the support beyond strain (*direct* support-induced effects). The direct effects result from charge transfer, polarization and chemisorption, and cause a significant increase in the Raman frequency of the Ni-supported *h*-BN.

ACKNOWLEDGMENTS

J.O. acknowledges funding from Ecuador Government's agency SENESCYT in the form of a PhD studentship award (CA-2012-2). This work made use of ARCHER, the UK's national high-performance computing service, *via* the UK's HPC Materials Chemistry Consortium, which is funded by EPSRC (EP/L000202). The work of F.I and F.V. has been supported by the Spanish *Ministerio de Economía y Competitividad* (MINECO) through the CTQ2015-64618- R FEDER grant and, in part by the *Generalitat de Catalunya* through 2017SGR13 and XRQTC grants. F. V. thanks MINECO for a *Ramón y Cajal* (RYC-2012-10129) research contract and F.I. acknowledges additional support from 2015 ICREA Academia Award. Financial support from Spanish MICIUN through the Excellence *María de Maeztu* program (grant MDM-2017-0767) is also acknowledged.

REFERENCES

1 X. Liu, T. Duan, Y. Sui, C. Meng and Y. Han, *RSC Adv.*, 2014, **4**, 38750–38760.

2 K. Uosaki, G. Elumalai, H. Noguchi, T. Masuda, A. Lyalin, A. Nakayama and T. Taketsugu, *J. Am. Chem. Soc.*, 2014, **136**, 6542–6545.

3 S. Joshi, D. Ecija, R. Koitz, M. Iannuzzi, A. P. Seitsonen, J. Hutter, H. Sachdev, S. Vijayaraghavan, F. Bischoff, K. Seufert, J. V. Barth and W. Auwärter, *Nano Lett.*, 2012, **12**, 5821–5828.

4 K. K. Kim, A. Hsu, X. Jia, S. M. Kim, Y. Shi, M. Hofmann, D. Nezich, J. F. Rodriguez-Nieva, M. Dresselhaus, T. Palacios and J. Kong, *Nano Lett.*, 2012, **12**, 161–166.

5 A. B. Preobrajenski, A. S. Vinogradov, M. L. Ng, E. Ćavar, R. Westerström, A. Mikkelsen, E. Lundgren and N. Mårtensson, *Phys. Rev. B*, 2007, **75**, 245412.

6 M. Morscher, M. Corso, T. Greber and J. Osterwalder, *Surf. Sci.*, 2006, **600**, 3280–3284.

7 Y. Gao, W. Ren, T. Ma, Z. Liu, Y. Zhang, W.-B. Liu, L.-P. Ma, X. Ma and H.-M. Cheng, *ACS Nano*, 2013, **7**, 5199–5206.

8 F. Schulz, R. Drost, S. K. Hämäläinen, T. Demonchaux, A. P. Seitsonen and P. Liljeroth, *Phys. Rev. B*, 2014, **89**, 235429.

9 W. Auwärter, T. J. Kreutz, T. Greber and J. Osterwalder, *Surf. Sci.*, 1999, **429**, 229–236.

10 Y. Kubota, K. Watanabe, O. Tsuda and T. Taniguchi, *Science*, 2007, **317**, 932–4.

11 T. Sugino and T. Tai, *Jpn. J. Appl. Phys.*, 2000, **39**, L1101–L1104.

12 K. Watanabe, T. Taniguchi and H. Kanda, *Nat. Mater.*, 2004, **3**, 404–409.

13 A. H. M. A. Wasey, S. Chakrabarty, G. P. Das and C. Majumder, *ACS Appl. Mater. Interfaces*, 2013, **5**, 10404–10408.

14 S. Lin, J. Huang and X. Gao, *Phys. Chem. Chem. Phys.*, 2015, **17**, 22097–22105.

15 X. Gao, S. Wang and S. Lin, *ACS Appl. Mater. Interfaces*, 2016, **8**, 24238–24247.

16 E. Rokuta, Y. Hasegawa, K. Suzuki, Y. Gamou, C. Oshima and A. Nagashima, *Phys. Rev. Lett.*, 1997, **79**, 4609–4612.

17 A. B. Preobrajenski, A. S. Vinogradov and N. Mårtensson, *Surf. Sci.*, 2005, **582**, 21–30.

18 A. B. Preobrajenski, S. A. Krasnikov, A. S. Vinogradov, M. L. Ng, T. Käämbre, A. A. Cafolla and N. Mårtensson, *Phys. Rev. B*, 2008, **77**, 085421.

19 J. Gómez Díaz, Y. Ding, R. Koitz, A. P. Seitsonen, M. Iannuzzi and J. Hutter, *Theor. Chem. Acc.*, 2013, **132**, 1350.

20 R. W. G. Wyckoff, *Crystal Structures, Volume 1*, Interscience Publishers, New York, Second., 1963.

21 W. Paszkowicz, J. B. Pelka, M. Knapp, T. Szyszko and S. Podsiadlo, *Appl. Phys. A Mater. Sci. Process.*, 2002, **75**, 431–435.

22 R. V. Gorbachev, I. Riaz, R. R. Nair, R. Jalil, L. Britnell, B. D. Belle, E. W. Hill, K. S. Novoselov, K. Watanabe, T. Taniguchi, A. K. Geim and P. Blake, *Small*, 2011, **7**, 465–8.

23 G. Kresse and J. Furthmüller, *Comput. Mater. Sci.*, 1996, **6**, 15–50.

24 G. Kresse and J. Furthmüller, *Phys. Rev. B*, 1996, **54**, 11169–11186.

25 P. E. Blöchl, *Phys. Rev. B*, 1994, **50**, 17953–17979.

26 G. Kresse and D. Joubert, *Phys. Rev. B*, 1999, **59**, 1758–1775.

27 H. J. Monkhorst and J. D. Pack, *Phys. Rev. B*, 1976, **13**, 5188–5192.

28 G. Makov and M. Payne, *Phys. Rev. B*, 1995, **51**, 4014–4022.

29 W. Zhao, S. M. Kozlov, O. Höfert, K. Gotterbarm, M. P. A. Lorenz, F. Viñes, C. Papp, A. Görling and H. P. Steinrück, *J. Phys. Chem. Lett.*, 2011, **2**, 759–764.

30 Y. Gamou, M. Terai, A. Nagashima and C. Oshima, *Sci. Reports Rerearch Institutes Tohoku Univ. Ser. A-Physics*, 1997, **44**, 211–214.

31 J. P. Perdew, K. Burke and M. Ernzerhof, *Phys. Rev. Lett.*, 1996, **77**, 3865–3868.

32 S. Grimme, *J. Comput. Chem.*, 2006, **27**, 1787–99.

33 S. Grimme, J. Antony, S. Ehrlich and H. Krieg, *J. Chem. Phys.*, 2010, **132**, 154104.

34 J. Klimeš, D. R. Bowler and A. Michaelides, *J. Phys. Condens. Matter*, 2010, **22**, 022201.

35 J. Klimeš, D. R. Bowler and A. Michaelides, *Phys. Rev. B*, 2011, **83**, 195131.

36 G. Mills, H. Jónsson and G. K. Schenter, *Surf. Sci.*, 1995, **324**, 305–337.

37 A. A. Tonkikh, E. N. Voloshina, P. Werner, H. Blumtritt, B. Senkovskiy, G. Güntherodt, S. S. P. Parkin and Y. S. Dedkov, *Sci. Rep.*, 2016, **6**, 23547.

38 M. Muntwiler, W. Auwärter, F. Baumberger, M. Hoesch, T. Greber and J. Osterwalder, *Surf. Sci.*, 2001, **472**, 125–132.

39 J. Osterwalder, W. Auwärter, M. Muntwiler and T. Greber, *e-Journal Surf. Sci. Nanotechnol.*, 2003, **1**, 124–129.

40 P. Janthon, F. Viñes, S. M. Kozlov, J. Limtrakul and F. Illas, *J. Chem. Phys.*, 2013, **138**, 244701.

41 A. Nagashima, N. Tejima, Y. Gamou, T. Kawai and C. Oshima, *Phys. Rev. Lett.*, 1995, **75**, 3918–3921.

42 A. Nagashima, N. Tejima, Y. Gamou, T. Kawai and C. Oshima, *Phys. Rev. B*, 1995, **51**, 4606–4613.

43 A. Nagashima, N. Tejima, Y. Gamou, T. Kawai and C. Oshima, *Surf. Sci.*, 1996, **357**–**358**, 307–311.

44 A. Nagashima, N. Tejima, Y. Gamou, T. Kawai, M. Terai, M. Wakabayashi and C. Oshima, *Int. J. Mod. Phys. B*, 1996, **10**, 3517–3537.

45 B. Grad, P. Blaha, K. Schwarz, W. Auwärter and T. Greber, *Phys. Rev. B*, 2003, **68**, 085404.

46 R. Laskowski, P. Blaha and K. Schwarz, *Phys. Rev. B*, 2008, **78**, 045409.

47 M. N. Huda and L. Kleinman, *Phys. Rev. B*, 2006, **74**, 075418.

48 A. Ebnonnasir, S. Kodambaka and C. V. Ciobanu, *Surf. Rev. Lett.*, 2015, **22**, 1550078.

49 P. Ares, E. G. Michel, M. Pisarra, P. Segovia, C. Gómez-Navarro, F. Martín, J. Gómez-Herrero, F. Zamora and C. Díaz, *Adv. Funct. Mater.*, 2019, **29**, 1806715.

50 V. G. Ruiz, W. Liu, E. Zojer, M. Scheffler and A. Tkatchenko, *Phys. Rev. Lett.*, 2012, **108**, 146103.

51 W. Liu, J. Carrasco, B. Santra, A. Michaelides, M. Scheffler and A. Tkatchenko, *Phys. Rev. B*, 2012, **86**, 245405.

52 J. Carrasco, W. Liu, A. Michaelides and A. Tkatchenko, *J. Chem. Phys.*, 2014, **140**, 084704.

53 J. Ontaneda, A. Singh, U. V Waghmare and R. Grau-Crespo, *J. Phys. Condens. Matter*, 2018, **30**, 185701.